

In-plane Schottky-barrier field-effect transistors with a 4-nm channel based on 1T/2H MoTe₂ and WTe₂

Cite as: AIP Advances **11**, 065316 (2021); <https://doi.org/10.1063/5.0054348>
Submitted: 22 April 2021 • Accepted: 25 May 2021 • Published Online: 11 June 2021

Houping Yang, Yueyue Tian,  Junjun Li, et al.

COLLECTIONS

 This paper was selected as an Editor's Pick



View Online



Export Citation



CrossMark

ARTICLES YOU MAY BE INTERESTED IN

[Gate-tunable van der Waals heterostructure based on semimetallic WTe₂ and semiconducting MoTe₂](#)

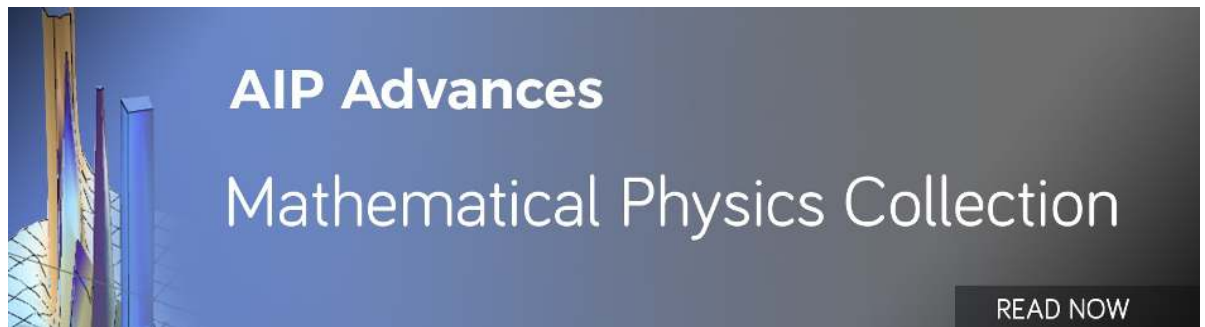
Applied Physics Letters **118**, 133103 (2021); <https://doi.org/10.1063/5.0046207>

[Band alignment of two-dimensional transition metal dichalcogenides: Application in tunnel field effect transistors](#)

Applied Physics Letters **103**, 053513 (2013); <https://doi.org/10.1063/1.4817409>

[How good are 2D transistors? An application-specific benchmarking study](#)

Applied Physics Letters **118**, 030501 (2021); <https://doi.org/10.1063/5.0029712>



AIP Advances
Mathematical Physics Collection

[READ NOW](#)

In-plane Schottky-barrier field-effect transistors with a 4-nm channel based on 1T/2H MoTe₂ and WTe₂

Cite as: AIP Advances 11, 065316 (2021); doi: 10.1063/5.0054348

Submitted: 22 April 2021 • Accepted: 25 May 2021 •

Published Online: 11 June 2021



Houping Yang,¹ Yueyue Tian,¹ Junjun Li,²  Yiqun Xie,³  Wei Ren,^{1,4}  and Yin Wang^{1,2,a)} 

AFFILIATIONS

¹International Centre for Quantum and Molecular Structures and Department of Physics, Shanghai University, Shanghai 200444, China

²Hongzhiwei Technology (Shanghai) Co., Ltd., Shanghai 201206, China

³Department of Physics, Shanghai Normal University, 100 Guilin Road, Shanghai 200232, China

⁴Materials Genome Institute, State Key Laboratory of Advanced Special Steel, Shanghai Key Laboratory of High Temperature Superconductors, Shanghai University, Shanghai 200444, China

^{a)}Author to whom correspondence should be addressed: yinwang@shu.edu.cn

ABSTRACT

As state-of-the-art fabrication techniques are approaching the 3 nm size, the traditional silicon-based circuit faces huge challenges. Transistors based on two-dimensional (2D) materials have attracted much attention as potential alternative candidates. However, critical performances including the subthreshold swing (SS), on/off ratio, and magnitude of the on-state current for 2D transistors around 3 nm size are far less to be studied well. In this work, we propose in-plane Schottky-barrier field-effect transistors (SBFETs) with a 4-nm channel based on the lateral heterostructure of monolayer 1T/2H MoTe₂ and WTe₂. The electric transport properties are investigated by first-principles quantum transport simulations. At a 0.64 V bias, the WTe₂ SBFET has an on-state current of 3861 $\mu\text{A}/\mu\text{m}$, with a 4.5×10^4 on/off ratio and an SS of 87 mV/dec, while the MoTe₂ SBFET has an on-state current of 1480 $\mu\text{A}/\mu\text{m}$, with a large on/off rate of 3.6×10^5 and an SS of 78 mV/dec. Our results suggest that FETs based on the lateral heterostructure of 1T/2H MoTe₂ (WTe₂) are promising candidates for high-performance 2D transistors.

© 2021 Author(s). All article content, except where otherwise noted, is licensed under a Creative Commons Attribution (CC BY) license (<http://creativecommons.org/licenses/by/4.0/>). <https://doi.org/10.1063/5.0054348>

I. INTRODUCTION

As the progress of Moore's law has slowed down, silicon-based integrated circuits that have been developed rapidly for decades face new challenges. As device nodes are gradually reduced to 5 nm, severe short channel effects will prevent continued miniaturization of semiconductor silicon-based electronic transistors.^{1,2} According to the International Semiconductor Technology Roadmap (ITRS), two-dimensional (2D) semiconductor materials such as graphene, phosphorus, and transition metal disulfides (TMDs) are considered to be candidates for final channel materials that can extend the transistor to the sub-5 nm range.³⁻⁹ They have a thin atomic thickness; therefore, an ideal gate control can be achieved by reducing the short channel effect and leakage current of the field effect transistor (FET).^{10,11} Among these 2D materials, monolayer TMDs are highly

attractive because of their excellent optical, electronic, mechanical, and chemical properties.^{12,13} TMDs have unique advantages over several other 2D materials. For example, compared to gapless graphene,¹⁴ monolayer TMDs have a direct bandgap (1.0–2.0 eV),¹⁵ which is necessary for the channel of a semiconductor device. Compared to black phosphorus,¹⁶ TMDs have a better environmental stability.

Encouraged by the rapid development of sub-5 nm technology, it is highly desirable to know whether the excellent device performance of monolayer TMD FETs can be maintained when the gate length is reduced to less than 5 nm.¹⁷ Experimentally, a MoS₂ transistor with a gate length of 1 nm has been successfully fabricated,¹⁸ with a near ideal subthreshold swing (SS) of 65 mV/dec and an on/off current ratio of 10^6 ; however, the on-current is relatively small—10 $\mu\text{A}/\mu\text{m}$. A large amount of theoretical work has studied

the performance limits of sub-5 nm transistors. For example, Quhe *et al.* found that the monolayer ReS₂ transistor has an excellent gate characteristic with an SS of 52–72 mV/dec when the gate length shortens to 5 nm.¹⁹ Li *et al.* simulated a tunneling field effect transistor composed of monolayer black phosphorous, which has an SS of 90 mV/dec and an on-current of 1123 $\mu\text{A}/\mu\text{m}$.¹⁷ Fan *et al.* studied the 2D TMD FET with a 8.8 nm gate length²⁰ and found that the WTe₂-FET has a high on-state current of 1729 $\mu\text{A}/\mu\text{m}$.

In this paper, we investigate the electronic transport properties of monolayer MoTe₂ and WTe₂ Schottky-barrier field-effect transistors (SBFETs) based on the 1T/2H contact with a channel length of about 4 nm using first-principles quantum transport simulations. A good SS of around 80 mV/dec, high on/off ratio (10^4), and large on-current ($10^4 \mu\text{A}/\mu\text{m}$) are simultaneously achieved, indicating an outstanding performance within the sub-5 nm size for MoTe₂ and WTe₂ SBFETs.

II. MODEL AND METHODS

It has been shown that both monolayer WTe₂ and MoTe₂ have 1T and 2H phases, as shown in Figs. 1(a)–1(d). Here, we construct the in-plane heterostructure with a 1T/2H/1T configuration for both monolayer WTe₂ and MoTe₂, where the 1T/2H junctions are connected along the armchair direction, as shown in Fig. 1(e). Similar in-plane 1T/2H/1T MoS₂ SBFETs have been assembled in a recent experiment.²¹ Figures 1(a) and 1(b) show the atomic structure of semiconductor (2H) and metal (1T) phases for monolayer MoTe₂. The lattice constants of 2H-phase MoTe₂ are $a = 3.553 \text{ \AA}$ and $b = 6.10 \text{ \AA}$, which are in good agreement with experimental measurements and other theoretical calculations.^{20,22} The primitive cell of monolayer MoTe₂ contains one Mo atom and a pair of Te atoms. In the 2H phase, Te atoms in the upper layer lies directly on top of

the Te atoms in the bottom sublayer, with an AB stacked sequence. The 1T phase has an ABC atomic stacked sequence, where Te atoms in the upper and lower sublayers are offset from each other and Mo atoms occupy the hexagon holes of the Te layers. The top view of the MoTe₂ 1T/2H/1T-SBFET is shown in Fig. 1(e), and the schematic diagram is shown in Fig. 1(f). The SBFET consists of sources and drains composed of a metallic 1T phase, which extends to $\pm z$, respectively. A scattering region composed of monolayer 2H-MoTe₂ connects the source and drain, with a (channel) length (L_g) of 4 nm. On the top and bottom of the 2H-MoTe₂, equivalent oxides with a thickness (EOT) of 0.41 nm and a power supply voltage ($V_{ds} = 0.64 \text{ V}$) are added, following ITRS high performance (HP) requirements.²³ The potential of the central region is controlled by double gate voltage (V_g). The current flows along the z -direction, namely, the zigzag direction. The periodic boundary condition is satisfied in the x direction, and to avoid interactions between periodic replicas, a vacuum layer of 30 \AA is added in the y direction.

The electric current is calculated using the nonequilibrium Green's function formalisms²⁴ combined with density-functional theory (NEGF-DFT), as implemented in the first-principles quantum transport package *NanoDcal*.^{25–27} Standard norm-conserving nonlocal pseudopotentials²⁸ are used to define the atomic cores, a double zeta polarization (DZP) linear combination of the atomic orbital basis set is used to expand physical quantities,²⁹ and the exchange–correlation potential is treated at the local density approximation (LDA) level. The k -point samplings for self-consistent calculations are $8 \times 1 \times 100$. When a bias voltage is applied, the drain current I_d at different gate voltages can be obtained by the Landauer formula,³⁰

$$I_d(V_{ds}, V_g) = \frac{2e}{h} \int T(E, V_{ds}, V_g) \times [f_L(E - \mu_L) - f_R(E - \mu_R)] dE, \quad (1)$$

where V_{ds} is the power supply voltage, V_g is the gate voltage, $T(E, V_{ds}, V_g)$ is the transmission coefficient, μ_L and μ_R are the electrochemical potential of the left and right electrodes, and f_L and f_R are the Fermi–Dirac distribution functions of the left and right electrodes, respectively.

III. RESULTS AND DISCUSSIONS

Electronic band structures of monolayer MoTe₂ and WTe₂ are shown in Fig. 2. For 2H MoTe₂ and WTe₂, the direct bandgaps are 1.12 and 1.08 eV, respectively, while their 1T phases are evidently metallic. Next, we calculated the effective masses of 2H MoTe₂ and WTe₂ as listed in Table I, which agree well with the previous reports.^{31,32} Furthermore, we found that there is a band offset in the 1T/2H junction, which is in good agreement with previous theoretical calculations.^{20,33} The 1T/2H interface causes the band-bending of monolayer 2H MoTe₂ (WTe₂) in the scattering region as it is essentially a metal–semiconductor contact. Consequently, a Schottky barrier (SB, Φ_{SB}) is induced at the interface, which plays an important role in determining the transport properties of the SBFETs. A recent theoretical study has proposed a method to calculate the SB for the metal–semiconductor junction.³⁴ Following their method, we calculate Φ_{SB} for the MoTe₂ SBFET, which is discussed below as an example. First, we obtain the energy difference

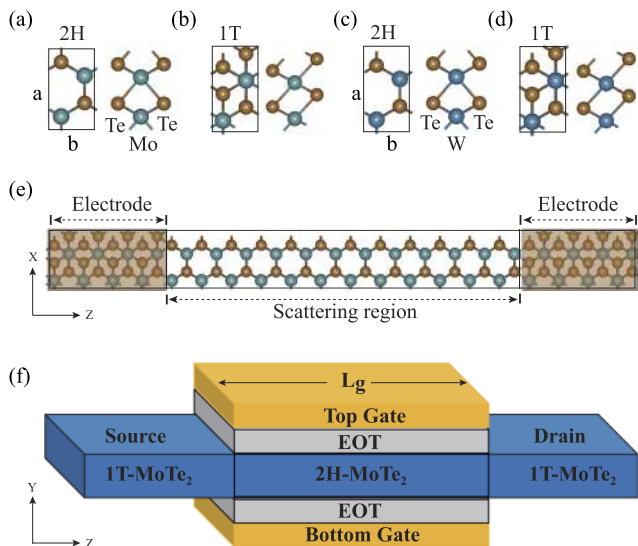


FIG. 1. Top and side views of the atomic structures of (a) and (b) monolayer MoTe₂ and (c) and (d) WTe₂ with 2H and 1T phases, respectively. (e) The top view of the 1T/2H/1T SBFET configuration, and (f) the schematic diagram of the 1T/2H/1T SBFET with double gates.

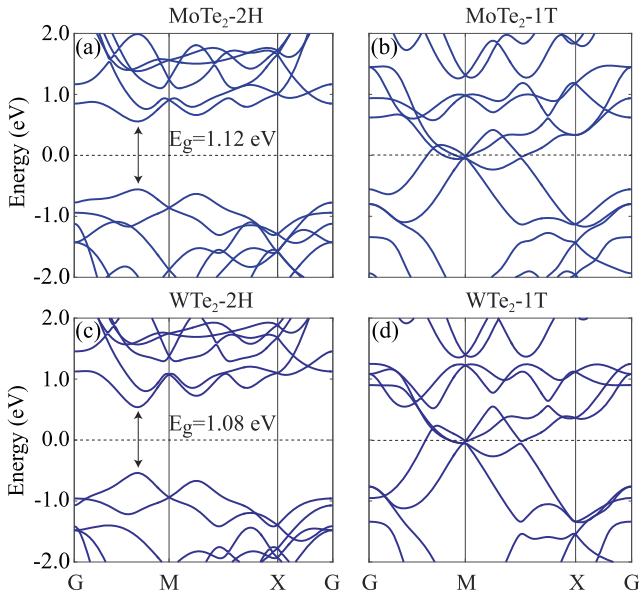


FIG. 2. Electronic bandstructure of (a) and (b) monolayer MoTe₂ and (c) and (d) WTe₂ with 2H and 1T phases.

E_{FC} (0.35 eV) between the Fermi level (0 eV) and the conduction band minimum (CBM) from the projected density of states (PDOS) and the electron transmission spectrum of the device, as indicated in Fig. 3(a). Then, the difference in the macroscopic average potential V_{macro} along the z -direction between the 1T and 2H MoTe₂ junction in the SBFET is calculated, which is $\Delta V = 0.02$ eV, as shown in Fig. 3(b). Consequently, we obtain $\Phi_{SB} = E_{FC} + \Delta V = 0.37$ eV. Φ_{SB} for the WTe₂ SBFET is also calculated in a similar way, which is 0.34 eV. Moreover, from the PDOS shown in Fig. 3(a), we can see that the band alignment is similar to that between metal and n-type semiconductors since the Fermi level is closer to the conduction band minimum (CBM) of 2H MoTe₂.

Having studied the band alignments of the 1T/2H/1T SBFET, we next investigate the electric current at a bias voltage, which can be controlled by a gate voltage (V_g). The smaller the SS of the FET, the better the gate control capability,¹⁷ according to its definition $\frac{\partial V_g}{\partial \log I_d}$, where I_d is the drain current. For conventional FETs, the theoretical limit of the SS is 60 mV/dec. In general, it will increase with the reduction in the physical gate length because of the increased short

TABLE I. Effective mass of electrons m_n^x (m_n^y) and holes m_p^x (m_p^y) along the transverse (longitudinal) directions of 2H MoTe₂ and WTe₂. The unit of effective mass is the rest mass of electron m_0 .

	MoTe ₂	MoTe ₂ ³¹	MoTe ₂ ³²	WTe ₂	WTe ₂ ³¹
m_n^x	0.594	0.553	0.616	0.327	0.313
m_n^y	0.595	0.552	0.603	0.327	0.299
m_p^x	0.737	0.666	0.758	0.428	0.384
m_p^y	0.739	0.668	0.740	0.427	0.420

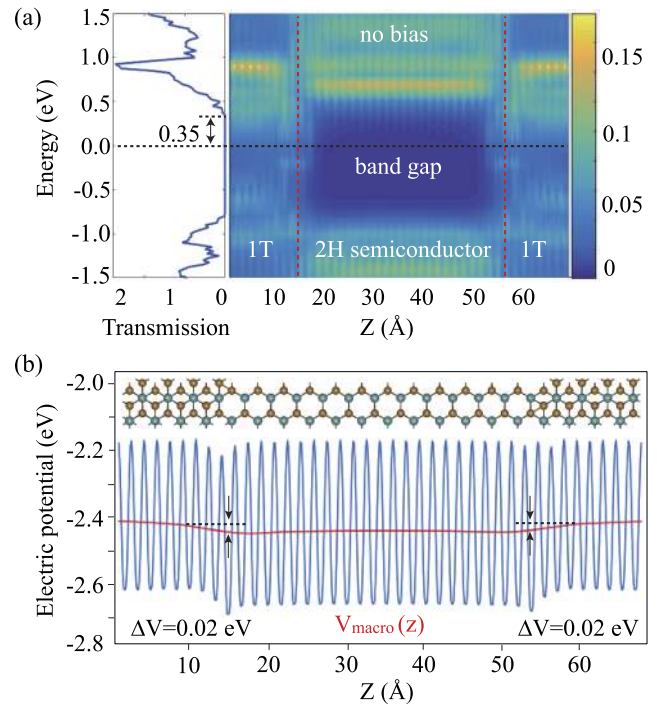


FIG. 3. (a) Transmission spectrum and the projected density of state of the MoTe₂ 1T/2H/1T-SBFET. The Fermi energy at 0 eV is indicated by a black dashed line. (b) The electric potential (in blue) and the macroscopic average potential V_{macro} (in red) of the SBFET along the transport z -direction.

channel effect. Figure 4 depicts the $(I_d - V_g)$ curves for both MoTe₂ and WTe₂ SBFETs. The bias voltage (V_{ds}) between the source and drain is set to 0.64 V, while both top and bottom V_g vary from 0 to 1.4 V with an interval of 0.1 V. It can be seen that the current

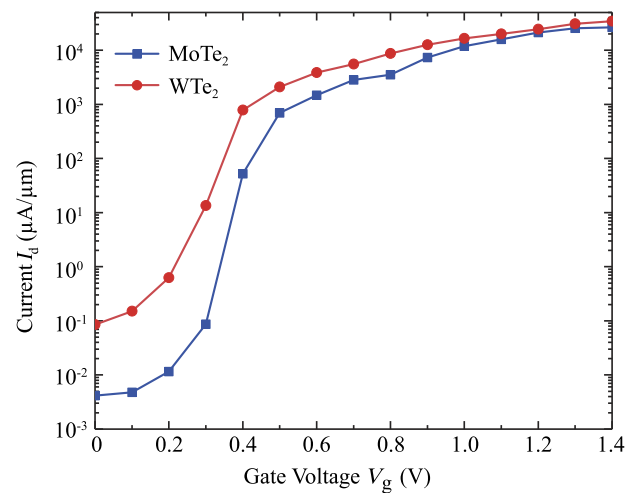


FIG. 4. Variation in the current with the gate voltage V_g for the MoTe₂ and WTe₂ SBFETs at a bias voltage of $V_{ds} = 0.64$ V.

TABLE II. The performances of the MoTe₂ and WTe₂ SBFETs compared with HP device requirements of the ITRS and other 2D materials.

FET	L_g (nm)	I_{on} ($\mu\text{A}/\mu\text{m}$)	I_{on}/I_{off}	SS (mV/dec)	Reference
ITRS HP	5.1	900	9×10^3	...	23
MoTe ₂	4	1480	3.6×10^5	78	This work
WTe ₂	4	3861	4.5×10^4	87	This work
ReS ₂	4	121	2.4×10^6	52	19
Sb	4	1483	1.5×10^4	118	35
Bi ₂ O ₂ Se	5	2067	2.1×10^4	111	36
BP	6	1574	1.2×10^4	56	37
BiN	8	724	7.1×10^3	73	38

I_d is 0.1 and 0.005 $\mu\text{A}/\mu\text{m}$ at $V_g = 0$ V for the WTe₂ and MoTe₂ SBFETs, respectively. The current increases gradually from $V_g = 0.1$ to 0.2 V; thereafter, it increases dramatically until 0.5 V and then gradually saturates from about 0.6 V. According to these two curves, the SS is calculated, which is 87 and 78 mV/dec for the WTe₂ and MoTe₂ SBFETs, respectively, close to the theoretical threshold of 60 mV/dec. We next discuss the on-state current I_{on} , which is an

important figure of merit for 2D FETs. Here, I_{on} is obtained at $V_g = 0.64$ V. The maximal drain current decreases as the SB height increases. I_{on} is bigger for the WTe₂ SBFET because of smaller Φ_{SB} . All I_{on} are illustrated in Table II. Noticeably, I_{on} is considerably large, which is 1480 $\mu\text{A}/\mu\text{m}$ (MoTe₂) and 3861 $\mu\text{A}/\mu\text{m}$ (WTe₂), with a large on/off ratio of 3.6×10^5 (MoTe₂) and 4.5×10^4 (WTe₂), which is higher than the ITRS HP requirement.

To better understand the (I_d - V_g) curves of these SBFETs, we calculated the transmission spectrum and PDOS for the two SBFETs at different V_g . Those for the MoTe₂ are presented in Fig. 5 as examples. It can be seen that, at zero V_g , the Fermi level is located in the bandgap of the 2H semiconductor, below the conduction bands. This means that the device is not conductive, only a tiny tunneling current flows in the device through the large SB, and the device is in an off-state. When a positive gate voltage is applied, the energy levels in the center region of the device shift downward with respect to the Fermi level, and at the same time, the shape of the SB is changed to a gradually shortened length. Consequently, the tunneling current is largely increased. At $V_g = 0.4$ V, conduction bands in the center region moves further downward, with the Fermi energy located in the conduction bands, which can be seen in the PDOS [Fig. 5(c)] and in the electron transmission spectrum [Fig. 5(e)]. This means that the conduction channels are opened, and therefore, the current is dramatically increased.

For comparison, we give the SS, on-state current I_{on} , and on/off ratio I_{on}/I_{off} for both the WTe₂ and MoTe₂ SBFETs in Table II. It can be seen that the WTe₂ SBFET has a larger on-state current than the MoTe₂ SBFET; however, it has a smaller on/off ratio and larger SS (87), which means less efficiency in tunneling the current by gate voltage. Overall, WTe₂ has a considerably large on-state current, which is much larger than that of several FETs based on other 2D materials,^{35–38} e.g., black phosphorous and ReS₂, while it also has a good SS and large on/off ratio, as shown in Table II. In contrast, the on-state currents of Bi₂O₂Se and antimonene are higher than that of MoTe₂, yet their SS and on/off ratio is smaller. Moreover, the on/off ratio and on-state currents of both the WTe₂ and MoTe₂ SBFETs satisfy the ITRS requirements for HP devices, and therefore, they are promising candidates for high-performance 2D transistors.

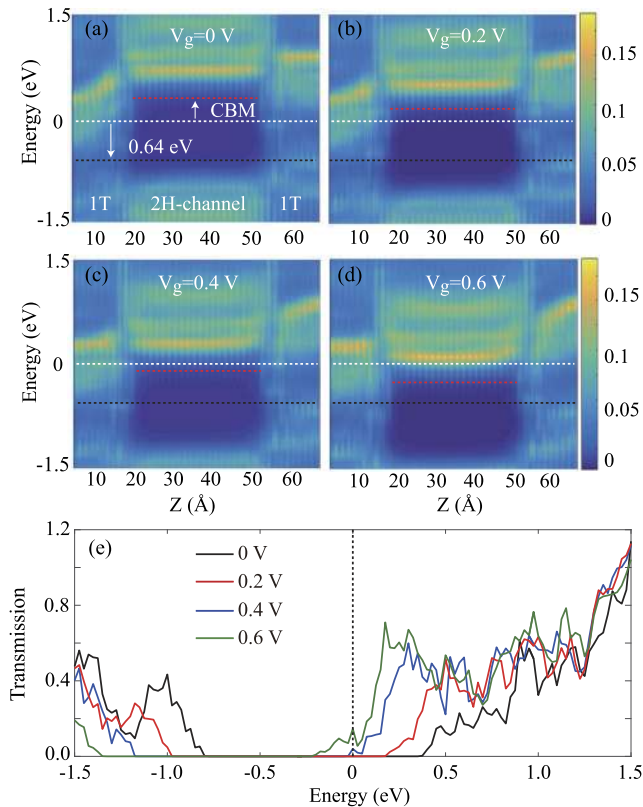


FIG. 5. (a)–(d) The projected density of states (PDOS) at $V_g = 0, 0.2, 0.4,$ and 0.6 V along the z -direction for the 1T/2H/1T MoTe₂ SBFET. White dashed lines indicate the Fermi level, and red dashed lines indicate the CBM. The transport window is indicated between the white and black dashed lines. (e) Electron transmission spectrum at $V_g = 0, 0.2, 0.4,$ and 0.6 V.

IV. CONCLUSION

In conclusion, we have investigated the gate-tuned electric transport properties of the 2D SBFETs of monolayer WTe₂ and

MoTe₂ with the 1T/2H/1T configuration by using first-principles quantum transport simulations. The MoTe₂ and WTe₂ SBFETs have a large on-state current of 1.5×10^3 and $3.8 \times 10^3 \mu\text{A}/\mu\text{m}$, with a good SS less than 90, and a high on/off ratio up to 10^5 . The on-state current can satisfy the ITRS requirements for HP devices and is larger than that of many other 2D-FETs ever reported. These results show that both WTe₂ and MoTe₂ SBFETs are promising candidates for high-performance 2D transistors in sub-5 nm size.

ACKNOWLEDGMENTS

H.Y. is grateful to Dr. Guodong Zhao and Ms. Mingyan Chen for useful discussions regarding the use of the *NanoDcal* software package. This work was financially supported by the National Key R&D Program of China (Grant No. 2018YFB040760) and the National Natural Science Foundation of China (Grant Nos. 11774217 and 11804216). H.Y. and Y.T. were partially supported by the Postgraduate Research Opportunities Program of Hongzhiwei Technology (Shanghai) Co. Ltd. (hzwtech-PROP).

DATA AVAILABILITY

The data that support the findings of this study are available from the corresponding author upon reasonable request.

REFERENCES

- ¹R. F. Service, *Science* **323**, 1000 (2009).
- ²A. D. Franklin, *Science* **349**, aab2750 (2015).
- ³G. Fiori, F. Bonaccorso, G. Iannaccone, T. Palacios, D. Neumaier, A. Seabaugh, S. K. Banerjee, and L. Colombo, *Nat. Nanotechnol.* **9**, 768 (2014).
- ⁴M. Chhowalla, D. Jena, and H. Zhang, *Nat. Rev. Mater.* **1**, 16052 (2016).
- ⁵F. Léonard and A. A. Talin, *Nat. Nanotechnol.* **6**, 773 (2011).
- ⁶A. Allain, J. Kang, K. Banerjee, and A. Kis, *Nat. Mater.* **14**, 1195 (2015).
- ⁷D. Akinwande, N. Petrone, and J. Hone, *Nat. Commun.* **5**, 5678 (2014).
- ⁸F. Schwierz, J. Pezoldt, and R. Granzner, *Nanoscale* **7**, 8261 (2015).
- ⁹W. Cao, J. Kang, D. Sarkar, W. Liu, and K. Banerjee, *IEEE Trans. Electron Devices* **62**, 3459 (2015).
- ¹⁰F. Schwierz, *Nat. Nanotechnol.* **5**, 487 (2010).
- ¹¹D. Sarkar, X. Xie, W. Liu, W. Cao, J. Kang, Y. Gong, S. Kraemer, P. M. Ajayan, and K. Banerjee, *Nature* **526**, 91 (2015).
- ¹²B. Radisavljevic, A. Radenovic, J. Brivio, V. Giacometti, and A. Kis, *Nat. Nanotechnol.* **6**, 147 (2011).
- ¹³Y. Yoon, K. Ganapathi, and S. Salahuddin, *Nano Lett.* **11**, 3768 (2011).
- ¹⁴A. H. Castro Neto, F. Guinea, N. M. R. Peres, K. S. Novoselov, and A. K. Geim, *Rev. Mod. Phys.* **81**, 109 (2009).
- ¹⁵Z.-Q. Fan, X.-W. Jiang, J. Chen, and J.-W. Luo, *ACS Appl. Mater. Interfaces* **10**, 19271 (2018).
- ¹⁶J. D. Wood, S. A. Wells, D. Jariwala, K.-S. Chen, E. Cho, V. K. Sangwan, X. Liu, L. J. Lauhon, T. J. Marks, and M. C. Hersam, *Nano Lett.* **14**, 6964 (2014).
- ¹⁷H. Li, B. Shi, Y. Pan, J. Li, L. Xu, L. Xu, Z. Zhang, F. Pan, and J. Lu, *Nanotechnology* **29**, 485202 (2018).
- ¹⁸S. B. Desai, S. R. Madhvapathy, A. B. Sachid, J. P. Llinas, Q. Wang, G. H. Ahn, G. Pitner, M. J. Kim, J. Bokor, C. Hu, H. S. P. Wong, and A. Javey, *Science* **354**, 99 (2016).
- ¹⁹R. Quhe, J. Chen, and J. Lu, *J. Mater. Chem. C* **7**, 1604 (2019).
- ²⁰Z.-Q. Fan, X.-W. Jiang, J.-W. Luo, L.-Y. Jiao, R. Huang, S.-S. Li, and L.-W. Wang, *Phys. Rev. B* **96**, 165402 (2017).
- ²¹Y. Katagiri, T. Nakamura, A. Ishii, C. Ohata, M. Hasegawa, S. Katsumoto, T. Cusati, A. Fortunelli, G. Iannaccone, G. Fiori, S. Roche, and J. Haryuyama, *Nano Lett.* **16**, 3788 (2016).
- ²²J. A. Wilson and A. D. Yoffe, *Adv. Phys.* **18**, 193 (1969).
- ²³See <http://www.itrs2.net/> for International Technology Roadmap for Semiconductors(ITRS).
- ²⁴A.-P. Jauho, N. S. Wingreen, and Y. Meir, *Phys. Rev. B* **50**, 5528 (1994).
- ²⁵J. Taylor, H. Guo, and J. Wang, *Phys. Rev. B* **63**, 245407 (2001).
- ²⁶J. Maassen, M. Harb, V. Michaud-Rioux, Y. Zhu, and H. Guo, *Proc. IEEE* **101**, 518 (2013).
- ²⁷See <http://www.hzwtech.com/> for details of transport package NanoDcal.
- ²⁸N. Troullier and J. L. Martins, *Phys. Rev. B* **43**, 1993 (1991).
- ²⁹J. M. Soler, E. Artacho, J. D. Gale, A. García, J. Junquera, P. Ordejón, and D. Sánchez-Portal, *J. Phys.: Condens. Matter* **14**, 2745 (2002).
- ³⁰M. Büttiker, Y. Imry, R. Landauer, and S. Pinhas, *Phys. Rev. B* **31**, 6207 (1985).
- ³¹P. Miró, M. Audiffred, and T. Heine, *Chem. Soc. Rev.* **43**, 6537 (2014).
- ³²L. Liu, S. B. Kumar, Y. Ouyang, and J. Guo, *IEEE Trans. Electron Devices* **58**, 3042 (2011).
- ³³Q. H. Wang, K. Kalantar-Zadeh, A. Kis, J. N. Coleman, and M. S. Strano, *Nat. Nanotechnol.* **7**, 699 (2012).
- ³⁴M. Aras, C. Kılıç, and S. Ciraci, *Phys. Rev. B* **95**, 075434 (2017).
- ³⁵Y. Yin, C. Shao, C. Zhang, Z. Zhang, X. Zhang, J. Robertson, and Y. Guo, *ACS Appl. Mater. Interfaces* **12**, 22378 (2020).
- ³⁶R. Quhe, J. Liu, J. Wu, J. Yang, Y. Wang, Q. Li, T. Li, Y. Guo, J. Yang, H. Peng, M. Lei, and J. Lu, *Nanoscale* **11**, 532 (2019).
- ³⁷H. Li, J. Tie, J. Li, M. Ye, H. Zhang, X. Zhang, Y. Pan, Y. Wang, R. Quhe, F. Pan, and J. Lu, *Nano Res.* **11**, 2658 (2018).
- ³⁸W. Zhou, S. Zhang, S. Guo, Y. Wang, J. Lu, X. Ming, Z. Li, H. Qu, and H. Zeng, *Phys. Rev. Appl.* **13**, 044066 (2020).